https://doi.org/10.5194/egusphere-2026-4948
Preprint. Discussion started: 21 August 2026

Molecular fingerprints reveal traffic $PM_{2.5}$ complexity beyond a controlled gasoline tailpipe molecular profile

Lijuan Li [a, b,c], Hongmei Xu [d], Xin Zhang [a, e], Qiyuan Wang [a], Hui Su [f], Fengxian Liu [c,g], Yang Chen [b], Yuemei Han [a,*], Junji Cao [a,h*]

[a] State Key Laboratory of Loess and Quaternary Geology, Institute of Earth Environment, Chinese Academy of Sciences, Xi'an 710061, China
[b] Chongqing Institute of Green and Intelligent Technology, Chinese Academy of Sciences, Chongqing 400714, China
[c] Shanxi Key Laboratory of Complex Air Pollution Control and Carbon Reduction, Taiyuan 030024, China
[d] Department of Environmental Science and Engineering, Xi'an Jiaotong University, Xi'an 710049, China
[e] School of Geography and Environment, Liaocheng University, Liaocheng 252000, China
[f] Xi'an Institute for Innovative Earth Environment Research, Xi'an 710061, China
[g] College of Environment and Ecology, Taiyuan University of Technology, Taiyuan 030024, China
[h] Institute of Atmospheric Physics, Chinese Academy of Sciences, Beijing 100029, China

[*] Corresponding authors: Yuemei Han (yuemei.han@ieecas.cn); Junji Cao (jjcao@mail.iap.ac.cn)

Abstract. Controlled gasoline tailpipe profiles may not fully represent traffic particulate matter with aerodynamic diameter ≤2.5 μm ($PM_{2.5}$) under real road conditions. The molecular compositions of tunnel and controlled tailpipe $PM_{2.5}$ were compared using high-resolution mass spectrometry. Formulas common to both profiles were concentrated at low *m/z* and low to intermediate carbon numbers and were dominated by CHO and CHON. In contrast, molecular formulas unique to the tunnel showed greater formula richness and had higher proportions of CHOS and CHONS formulas than those unique to the controlled tailpipe profile. Tailpipe coverage ratios were high for CHO and CHON formulas in both ionization modes (0.77–0.82 and 0.84–0.92, respectively) but much lower for the combined CHOS and CHONS class (0.10–0.15). Hierarchical clustering resolved a dominant shared CHO/CHON baseline and two smaller domains concentrated in tunnel samples, characterized respectively by organosulfur formulas and by candidate formulas associated with reported tire wear chemicals together with a low molecular mass CHN response in ESI+. Thus, the controlled gasoline tailpipe profile captured the dominant shared CHO/CHON molecular baseline but incompletely represented sulfur-rich and other chemically distinct molecular domains retained in tunnel aerosol. Comprehensive molecular characterization of traffic $PM_{2.5}$ therefore requires controlled tailpipe measurements together with molecular profiles representing non-tailpipe vehicle materials and near-road processing.

1 Introduction

Road traffic remains a chemically complex source of urban fine particulate matter ($PM_{2.5}$) with clear health relevance despite increasingly stringent exhaust controls (Boogaard et al., 2022; Zhong et al., 2017; Heydari et al., 2020). Traffic $PM_{2.5}$ integrates tailpipe exhaust with brake, tire, and road wear, lubricant and fuel related organics, resuspended road dust, and atmospheric

https://doi.org/10.5194/egusphere-2026-4948
Preprint. Discussion started: 21 August 2026

processing near roadways. Tailpipe exhaust contains gases and primary particulate matter, including elemental carbon (EC), organic particulate matter, and trace platinum group elements released from catalytic converters (Zuraski et al., 2025; Cunha-Lopes et al., 2023; Shafer et al., 2024). Non-exhaust sources may contribute roughly 20%–50% of $PM_{2.5}$ mass in near road environments, with the tire-wear fraction being particularly enriched in rubber-derived organics with reported toxicological activity, such as benzothiazoles, 6PPD, and 6PPD-quinone (Fussell et al., 2022; Jiang et al., 2024; Wu et al., 2026). After release, rapid dilution and cooling alter gas particle partitioning, while oxidation of volatile and semi-volatile traffic emissions promotes the formation of secondary organic aerosol (SOA), often yielding downwind organic aerosol (OA) concentrations that exceed directly emitted primary OA by factors of 3–15 (Platt et al., 2013; Fang et al., 2022; Schneider et al., 2024). These processes collectively reduce the specificity of bulk chemical indicators and limit the effectiveness of traditional receptor models based on averaged aerosol composition metrics.

Molecular characterization of traffic $PM_{2.5}$ has often relied on two approaches, chassis dynamometer testing and road/tunnel field sampling. The former isolates tailpipe emissions and provides reproducible measurements of primary particles under specified driving cycles. In contrast, tunnel measurements capture integrated real world fleet emissions including both tailpipe and non-exhaust particles (Cunha-Lopes et al., 2023; Yao et al., 2023). High-resolution mass spectrometry (HRMS) analyses applied to these two approaches have revealed distinct differences in molecular composition (Tong et al., 2016; Cui et al., 2019; Tang et al., 2020). Chassis dynamometer exhaust has been reported to be enriched in alkanes, monocyclic and bicyclic aromatics, polycyclic aromatic hydrocarbons, and nitroaromatics, whereas tunnel aerosols tend to contain larger fractions of oxidized organics and benzothiazoles (Alam et al., 2019; Tong et al., 2016). A recent study reported a higher SOA formation potential for a real world traffic mixture than for a dynamometer reconstruction (639 ± 156 vs 188 mg kg $fuel^{-1}$) (Zhang et al., 2024). This difference was attributed to a more diverse organic precursor mixture, non-tailpipe organic emissions, and high emitting events in the tunnel environment. These observations motivate a direct molecular assessment of the fraction of the tunnel profile represented by a controlled gasoline tailpipe profile and the chemically distinct domains retained under real road conditions.

Despite extensive characterization of traffic related organic aerosol, the extent to which a controlled single vehicle tailpipe profile represents the molecular composition of $PM_{2.5}$ under real road conditions remains poorly constrained. This study aimed to quantify the molecular coverage of tunnel aerosol by a controlled gasoline tailpipe profile and to identify chemically distinct molecular domains retained in the tunnel. $PM_{2.5}$ collected from an urban road tunnel was compared with tailpipe aerosol generated by one gasoline passenger vehicle under three steady chassis dynamometer conditions using UHPLC–ESI–HRMS. The controlled gasoline tailpipe profile was first characterized across the three operating conditions, while formulas detected in all 28 tunnel samples defined the persistent tunnel core. Tailpipe coverage ratios were calculated separately for each elemental class to quantify the extent to which tunnel HRMS peak area was associated with formulas also detected in the controlled profile. Kendrick mass defect analysis examined homologous organization within sulfur containing formulas, and reference guided screening identified candidate formulas associated with reported tire wear compounds. Volcano screening selected formulas with pronounced chassis dynamometer–tunnel differences, and HCA integrated their tunnel temporal

https://doi.org/10.5194/egusphere-2026-4948
Preprint. Discussion started: 21 August 2026

profiles with molecular descriptors to resolve the shared molecular baseline and the chemically distinct domains retained in tunnel aerosol.

2 Methodology

2.1 Controlled chassis dynamometer tailpipe aerosol sampling

Chassis dynamometer (CD) tests were conducted at the Xi'an Chengnan Vehicle Inspection Station to collect tailpipe $PM_{2.5}$ under three steady operating conditions. Although electrification is accelerating, vehicles with internal combustion engines still dominated China's automobile fleet in 2024. According to the Ministry of Public Security, new energy vehicles accounted for 8.90% of the national automobile stock at the end of 2024 (Ministry of Public Security of the People's Republic of China, 2025). A passenger car fueled with commercial RON 92 gasoline was operated on a two-roller chassis dynamometer at 0, 20, and 40 km h^{-1}. $PM_{2.5}$ filter sample was collected under each condition. Tailpipe exhaust was transferred through a microdilution channel positioned downstream of the tailpipe and directed to the sampling rack. Three MiniVol portable samplers (Airmetrics, USA) operated in parallel at 5 L min^{-1} each to collect $PM_{2.5}$ on one 47 mm polytetrafluoroethylene membrane filter and two 47 mm quartz fiber filters (Whatman). The quartz filters were extracted and analyzed by UHPLC–HRMS for organic molecular composition in this study.

2.2 Tunnel $PM_{2.5}$ sampling

Tunnel $PM_{2.5}$ samples were collected in the longest inner-city tunnel of Xi'an, China, from 2 to 8 August 2019, spanning Friday to the following Thursday. Sampling was conducted using a high-volume $PM_{2.5}$ air sampler (HVS-$PM_{2.5}$, Thermo-Anderson Inc.) operated at approximately 1.13 m^3 min^{-1}. Four 3 h sampling periods were used each day: 07:30–10:30 (Period I), 11:00–14:00 (Period II), 16:30–19:30 (Period III), and 20:00–23:00 (Period IV), all in local standard time. The sampling site and schedule were the same as those used in previous tunnel studies of PAHs and reactive oxygen species associated with $PM_{2.5}$ and of volatile organic compounds. Detailed procedures for tunnel $PM_{2.5}$ collection are described in those studies (Lei et al., 2022; Xu et al., 2021). The campaign yielded 28 valid tunnel samples and three field blanks. Within the designated urban control area, Xi'an enforced a weekday license-plate tail-number restriction from 07:00 to 20:00. The policy restricted two terminal digits per weekday, including temporary plates (Xinhua, 2019).

2.3 UHPLC–HRMS analysis

A quarter of each quartz fiber filter (4.3 cm^2 in area) was extracted three times by sonication for 15 min each using 5 mL of HPLC-grade acetonitrile (Fisher Scientific) per extraction. The combined extracts were filtered through a 0.2 μm PTFE membrane filter (13 mm diameter, Pall Co., USA) and concentrated to 1 mL under a gentle stream of nitrogen. Analyses were performed using a Vanquish Flex UHPLC system coupled to a Q Exactive Orbitrap mass spectrometer. Chromatographic

https://doi.org/10.5194/egusphere-2026-4948
Preprint. Discussion started: 21 August 2026

separation was conducted using a C18 column with a 55 min gradient at 30 °C. Full scan spectra were acquired in both negative and positive electrospray ionization (ESI) modes over *m/z* 50–750 at a resolving power of approximately 140,000 at *m/z* 200. Detailed chromatographic and ion source parameters followed Li et al. (2024a). Three field blanks underwent the same extraction and UHPLC–HRMS analysis as the tunnel samples. Peak areas were corrected for field blank contributions before all subsequent analyses.

2.4 Data processing

Raw UHPLC–HRMS data were processed using MZmine (v2.53) following the peak picking, chromatogram deconvolution, and retention time alignment workflow described by Zhang et al. (2025) and Lin et al. (2022). Molecular formulas were assigned separately to the aligned ESI− and ESI+ peak lists as $C_cH_hO_oN_nS_s$ using ^{12}C, ^{1}H, ^{16}O, ^{14}N, and ^{32}S, with atom number range of 1-40, 1-80, 0-50, 0-4, and 0-2, respectively. The mass tolerance for formula assignment was ±2 ppm for ESI− and ±3 ppm for ESI+. Candidate assignments were filtered using the nitrogen rule and O/C = 0–3, H/C = 0.3–3.0, S/C = 0–0.8, and N/C = 0–1.3. For chemical formula $C_cH_hO_oN_nS_s$, the average carbon oxidation state ($\overline{OS}_c$) of an organic molecule was computed as 2× O/C-H/C (Kroll et al., 2011). The modified aromaticity index (AI_{mod}) was calculated as $AI_{mod} = (1 + c - 0.5o - s - 0.5h - 0.5n)/(c - 0.5o - s - n)$ (Koch and Dittmar, 2006). The double-bond equivalent (DBE) reflects the degree of unsaturation of an organic molecule and was calculated as $(2 + 2c + n - h)/2$, assuming that nitrogen is trivalent and sulfur is divalent (Yassine et al., 2014; Kind and Fiehn, 2007). In addition, the Kendrick mass was calculated as $KM_{CH_2} = m_{exact} \times \frac{14}{14.01565}$, where m_{exact} is the monoisotopic exact mass of the assigned formula. The nominal Kendrick mass NKM_{CH_2} was obtained by rounding KM_{CH_2} to the nearest integer. The Kendrick mass defect was then calculated as $KMD_{CH_2} = NKM_{CH_2} - KM_{CH_2}$ (Kendrick, 1963).

2.5 Statistical analysis and hierarchical clustering

Volcano analysis was performed separately for ESI+ and ESI− to compare the tunnel samples with the CD samples. Each 3 h tunnel $PM_{2.5}$ filter sample was treated as one statistical unit, whereas the CD samples represented the three operating conditions of the same vehicle and were not independent vehicle replicates. Within each sample and ionization mode, blank-corrected peak areas were divided by the summed peak area of all assigned formulas to obtain within-mode relative peak areas. Formula–ionization-mode assignments were retained for hierarchical clustering analysis (HCA) when they were not classified as CD only, were detected in at least 10 of the 28 tunnel samples, and met the criteria of a nominal $p < 0.05$ from a two-sided Welch's *t* test and $|\log_2 FC| \geq 2$. This screening retained 709 assignments. Benjamini–Hochberg-adjusted q values were additionally calculated separately within each ionization mode as a multiple-testing check but were not used as the primary selection criterion. The data transformation, pseudocount, $\log_2 FC$ calculation, and multiple-testing results are described in Sect. S2 of the Supplement.

https://doi.org/10.5194/egusphere-2026-4948
Preprint. Discussion started: 21 August 2026

For HCA, the retained formula assignments were characterized using their temporal variation across the 28 tunnel samples and their molecular descriptors. Peak areas were normalized separately within ESI+ and ESI−, and a neutral formula detected in both modes was retained as a separate assignment in each mode. Temporal distances were derived from normalized peak area profiles, whereas chemical distances were calculated from O/C, H/C, and carbon number. After independent rescaling, the temporal and chemical distances were combined using the weighting parameter α and subjected to complete linkage agglomerative clustering. The $K = 3$ and $\alpha = 0.80$ solution was selected from $K = 3–6$ and $\alpha = 0.20–0.90$ based on silhouette diagnostics and the prespecified minimum domain size. Detailed data processing, distance construction, model selection, and parameter sensitivity analyses are provided in Sect. S3 of the Supplement.

3 Results and discussion

3.1. Molecular characteristics of the controlled gasoline tailpipe profile

The assigned molecular composition of the controlled gasoline tailpipe molecular profile differed among the three driving mode samples (Figure 1). In ESI− (ESI+) mode, the number of detected formulas was 662 (2,279) at idle, 582 (2,051) at 20 km h^{-1}, and 731 (2,379) at 40 km h^{-1}, with the lowest number observed at 20 km h^{-1}. This pattern indicates that the assigned tailpipe molecular profile varied among the three operating conditions. Comparable studies have shown that driving conditions and exhaust aftertreatment alter precursor emissions and aerosol composition (Pieber et al., 2018; Hartikainen et al., 2023; Paul et al., 2024). CHO and CHON together accounted for approximately 60% of the assigned formulas in both modes. In ESI−, the CHON number fraction increased from 29.0% at idle to 42.7% at 40 km h^{-1} accompanied by a decrease in CHO. This shift may reflect combined changes in emission strength, dilution, particle partitioning, and ESI response of nitrogen and oxygen containing organics across operating conditions (Rudnick, 2017). Sulfur-containing compounds (CHOS and CHONS) decreased from 37 % at idle to 26 % at 40 km h^{-1}, showing a lower contribution of sulfur containing formulas at the higher speed. The decrease is consistent with an operating condition dependent change in the detected contribution of fuel, lubricant, and additive related sulfur organics and their gas particle partitioning (Kim et al., 2016).

https://doi.org/10.5194/egusphere-2026-4948
Preprint. Discussion started: 21 August 2026

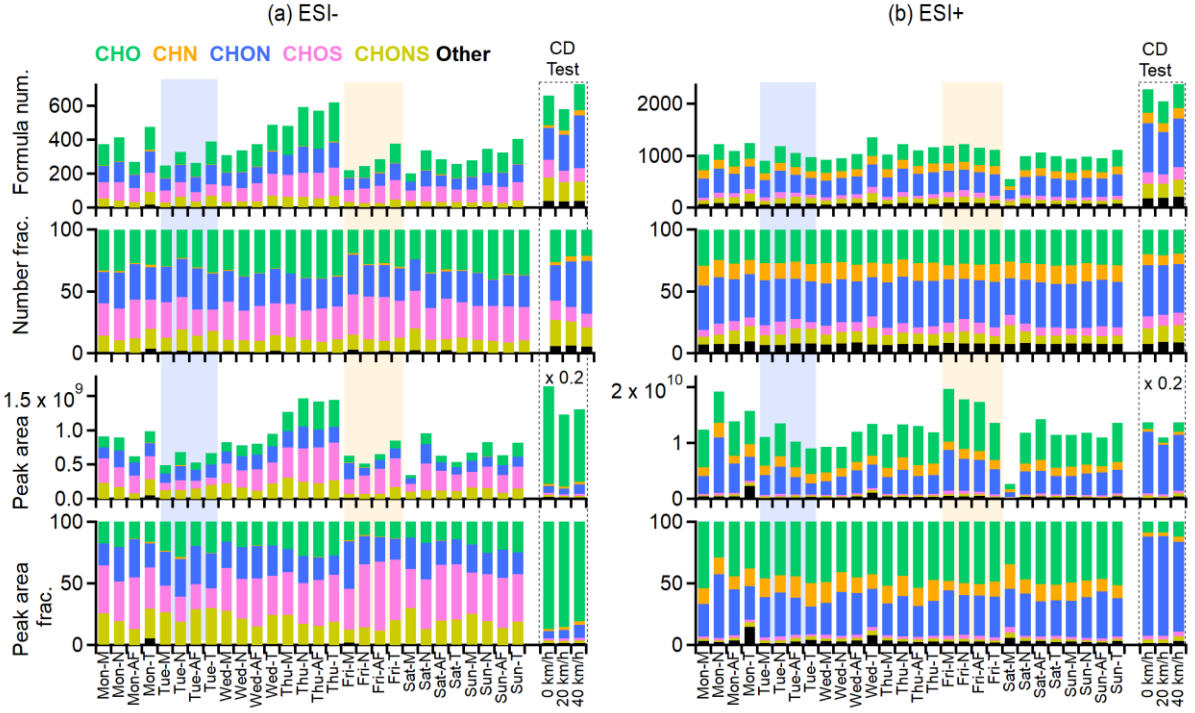

Figure 1. Molecular formula number and summed blank corrected HRMS peak area by elemental class (CHO, CHN, CHON, CHOS, CHONS, and Other) in (a) ESI− and (b) ESI+. Bar segments denote each class contribution to the sample total (upper rows by formula number, lower rows by peak area). Shaded bands indicate rainy periods (blue) and sunny periods (orange), and all other intervals are cloudy. The three rightmost bars in each panel denote the CD test samples. In the peak area panels, these three bars are scaled by a factor of 0.2.

Carbon number distributions varied between ionization modes and among operating conditions (Figure 2). Formulas detected in ESI− were characterized by lower carbon numbers (median nC = 12) than formulas detected in ESI+ (nC = 18). This contrast reflects ESI selectivity, with positive ion ESI favoring molecules with high proton affinity or basic functionalities and negative ion ESI favoring deprotonatable acidic and polar functionalities (Cech and Enke, 2001). From idle to 40 km h^{-1}, the median carbon number in ESI− decreased from 14 to 11, while the ESI+ distribution changed little. The lower carbon ESI− fraction showed greater compositional variation among the tested conditions than the higher carbon fraction prominent in ESI+. The persistence of higher carbon ESI+ formulas indicates a comparatively stable high carbon fraction in the controlled tailpipe molecular profile. This fraction may include lubricant or additive related constituents, consistent with previous evidence that lubricating oil contributes to organic particulate emissions from light duty gasoline vehicles and gasoline direct injection passenger cars (Worton et al., 2014; Sonntag et al., 2012; Pirjola et al., 2015).

https://doi.org/10.5194/egusphere-2026-4948
Preprint. Discussion started: 21 August 2026

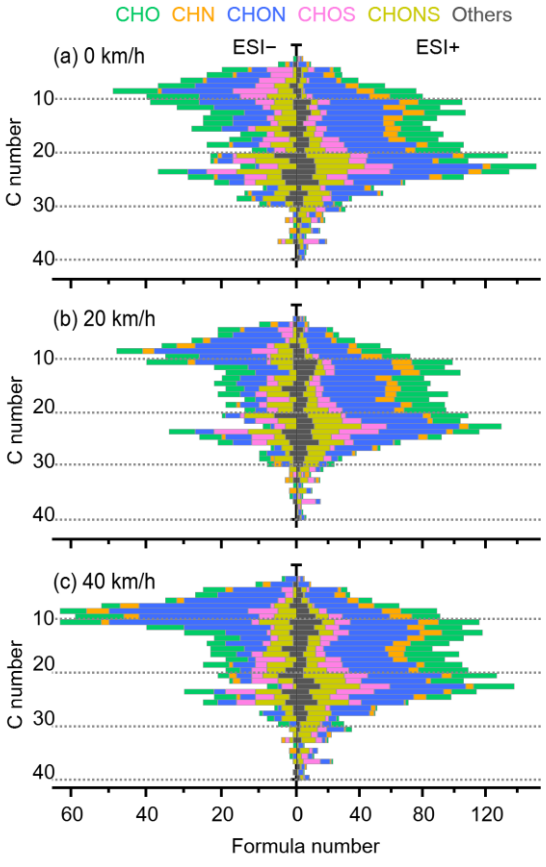

Figure 2. Carbon number distributions of assigned molecular formulas in controlled gasoline tailpipe aerosol collected at (a) 0 km h^{-1}, (b) 20 km h^{-1}, and (c) 40 km h^{-1}. Stacked horizontal bars denote the number of formulas by class (CHO, CHN, CHON, CHOS, CHONS, Others) within each carbon-number bin. ESI− is plotted to the left of the center line and ESI+ to the right.

Class resolved carbon number distributions of tailpipe organic formulas differed among driving modes and between ionization modes (Figure 2). The carbon number distributions of CHO and CHONS were relatively stable in both ionization modes, whereas CHON showed clearer variation across the three driving modes. In ESI−, CHON extended from C_5 to C_{15} with a maximum abundance near C_8, and the number of formulas in this range was approximately 60% higher at 40 km h^{-1} than at idle. In ESI+, CHON extended from C_{15} to C_{25}, and the fraction with carbon numbers below C_{20} increased by 15% from idle to 40 km h^{-1}. These changes show an expansion of lower carbon CHON formulas at 40 km h^{-1} across both ionization modes. Vehicle exhaust HRMS studies have similarly identified low carbon nitrogen containing formulas in positive ion spectra (He et al., 2025). In ESI+, the Other class was concentrated at high carbon numbers ($C_{>20}$) at idle and shifted toward lower carbon numbers at the higher speeds, with a peak near C_{10}. The high carbon distribution at idle is consistent with greater contributions

https://doi.org/10.5194/egusphere-2026-4948
Preprint. Discussion started: 21 August 2026

from incompletely combusted fuel constituents, including n-alkanes, and lubricant derived organics under low load operation. At the higher speed conditions, the shift toward shorter carbon chains may reflect the combined effects of reduced particle phase partitioning of semi-volatile long chain compounds together with thermal or oxidative fragmentation of fuel and lubricant derived organics (Worton et al., 2014).

Individual formulas were evaluated using the peak area ratio between operating conditions (defined as $R_{high/low}$ herein, e.g., $R_{40/0}$) to identify formulas with speed dependent changes in the controlled tailpipe molecular profile. Formulas with $R_{high/low} > 10^4$ were classified as emergent, and formulas with $R_{high/low} < 10^{-4}$were classified as attenuated. A nominal peak area of 1 was assigned when a formula was not detected in one of the two samples. Relative to idle, the 20 km h^{-1} profile showed attenuated to emergent formula ratios of 1.6 in ESI− and 1.8 in ESI+, while the 40 km h^{-1} profile showed ratios of 0.7 and 0.8, respectively (Table S1). CHON formed a major fraction of the emergent formulas. In ESI−, emergent CHON formulas shifted toward lower *m/z* and higher DBE/C in both speed contrasts. In ESI+, the 20/0 comparison was dominated by attenuated CHON formulas, while the 40/0 comparison contained concurrent emergence and attenuation, with emergent formulas again shifted toward lower *m/z* and higher DBE/C. These contrasts show that the detected distribution of nitrogen-containing formulas differed among the three tested conditions and define the compositional range of the controlled tailpipe profile.

3.2. Molecular fingerprints of tunnel traffic $PM_{2.5}$

Figure 1 presents the elemental class distributions based on assigned formula number and summed blank corrected HRMS peak area for tunnel aerosol extracts in (a) ESI− and (b) ESI+ modes. On average, more formulas were assigned in ESI+ than in ESI− (1,054 ± 150 vs 359 ± 112). A total of 294 neutral formulas occurred in both modes and accounted for approximately 25% of the peak area within each mode. Assigned formulas were grouped by elemental composition into CHO, CHN, CHON, CHOS, CHONS, and Other classes. In ESI− mode, sulfur-containing compounds (CHOS+CHONS) accounted for 39 ± 4% of formula numbers and 56 ± 7% of the total peak area, followed by CHO (32 ± 5%, 20 ± 5%), and CHON (27 ± 3 %, 24 ± 6%). This distribution contrasts with urban aerosol datasets commonly dominated by CHO and CHON in negative ion ESI (Wang et al., 2021). The high fraction of sulfur-containing compounds points to a distinct organosulfur rich HRMS response pattern in the tunnel aerosol (Tong et al., 2016; Tian et al., 2024). In ESI+, nitrogen-containing compounds (CHON + CHN) accounted for 49 ± 3% of formula number and 45 ± 5% of peak area, while CHO accounted for 27 ± 1% and 46 ± 6%, respectively. This polarity contrast therefore indicates complementary molecular response patterns, with protonatable nitrogen containing formulas contributing strongly in ESI+ and sulfur containing formulas accounting for a disproportionately large fraction of the ESI− peak area (Banerjee and Mazumdar, 2012).

https://doi.org/10.5194/egusphere-2026-4948
Preprint. Discussion started: 21 August 2026

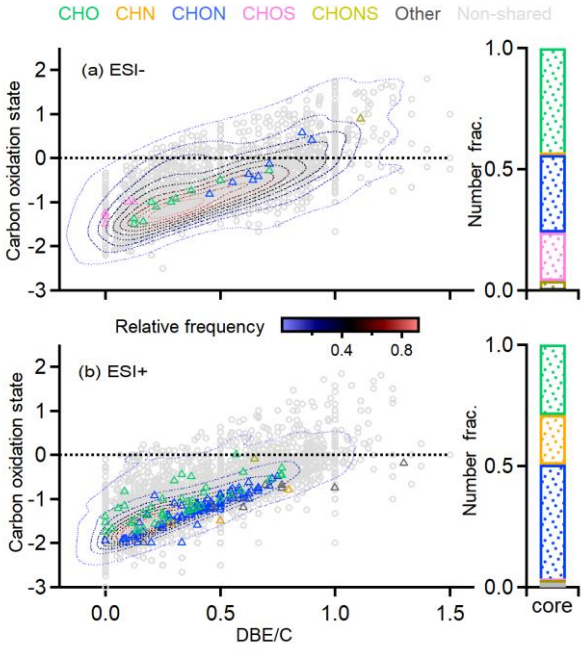

Figure 3. Average carbon oxidation state ($\overline{OS}_c$) versus DBE per carbon (DBE/C) for tunnel aerosol formulas in (a) ESI− and (b) ESI+. Colored triangles denote persistent core formulas detected in every sample and are colored by elemental class (CHO, CHN, CHON, CHOS, CHONS). Gray circles denote noncore formulas from all tunnel samples. Density contours show the distribution of all formulas, and stacked bars show the elemental class composition of each core group.

Persistent molecular formulas in tunnel aerosol were defined separately in each ionization mode as formulas detected in all 28 samples. The persistent core comprised 25 formulas in ESI− (156 in ESI+), representing 1% (3%) of all formulas detected in each mode, yet these species accounted for 29 % (40 %) of the average total peak area. Thus, a small recurrent formula group contributed disproportionately to the HRMS peak area, defining a persistent molecular baseline in the tunnel aerosol. In ESI−, the core formulas were dominated by CHO (44 %) and CHON (32 %) with sulfur-containing compounds contributing 24 %. Most of the core formulas (72 %) occupied a compact compositional region with mean $\overline{OS}_c$ of −0.70 ± 0.64 and mean DBE/C of 0.41 ± 0.31, indicating relatively reduced and lightly oxygenated composition (Figure 3). Given that approximately 80% of vehicles sampled in the tunnel were gasoline powered in this study (Figure S1), this persistent core is consistent with a stable molecular component of the gasoline dominated tunnel aerosol (Pieber et al., 2018; Worton et al., 2014; Tian et al., 2024). This component may integrate contributions from gasoline exhaust, lubricant related organics, tire wear related material, road dust, tunnel surface reservoirs, and in tunnel gas particle processing. In ESI+, nitrogen-containing compounds dominated the core, followed by CHO, and the $\overline{OS}_c$ -DBE/C distribution in compositional space was more diffuse than in ESI−. This pattern

https://doi.org/10.5194/egusphere-2026-4948
Preprint. Discussion started: 21 August 2026

is consistent with the preferential ESI+ detection of protonatable nitrogen containing organics and may reflect contributions from primary traffic emissions together with in tunnel processing of emitted organics under NO_x rich conditions (Wang et al., 2019; Cai et al., 2022).

Variation in the relative contribution of the persistent tunnel core was evaluated using one way ANOVA of CoreFrac, defined as the total peak area of persistent core formulas divided by the total peak area of all assigned organic formulas in each sample (Table S2). Formula number and total HRMS peak area were evaluated using the same analysis (Table S3). CoreFrac showed no significant variation among sampling periods or among the three sampled campaign days characterized by rainy, cloudy, and sunny conditions. Summed blank-corrected HRMS peak area differed among the three sampled campaign days in both ESI− ($F = 5.67$, $p = 0.026$) and ESI+ ($F = 10.27$, $p = 0.005$), whereas formula number showed no significant variation among sampling periods or among these three sampled days. In ESI−, mean total peak area was highest on the cloudy day, lowest on the rainy day, and intermediate on the sunny day. In ESI+, mean total peak area was highest on the sunny day and was approximately 50 % higher than on either the cloudy or rainy day. Together, these results indicate that the persistent tunnel core maintained a relatively consistent contribution to the detected molecular peak area even though the overall HRMS response varied among sampled days. Because each condition was represented by only one campaign day with four sampling periods, these comparisons describe day-specific variation during the campaign rather than general weather effects (Tong et al., 2016).

Relationships between bulk aerosol composition and HRMS molecular metrics were evaluated using Pearson correlation analysis with OC, EC, particulate NH_4^+, NO_3^-, and HRMS molecular classes (Figures S2 and S3). OC showed weak correlations with the HRMS composition, in contrast to many ambient datasets in which OC covaries with assigned formula number or total HRMS peak area (Li et al., 2024b; Lin et al., 2022). A plausible explanation is that tunnel OM contains substantial non-polar hydrocarbons from lubricating oil and fuel that dominate fresh vehicular POA, and these constituents are incompletely captured by ESI–HRMS (Worton et al., 2014). A limited subset of organic molecular formulas exhibited strong positive correlations ($r > 0.75$) with particulate NH_4^+ and NO_3^-. These formulas were dominated by CHO with a smaller CHOS contribution in ESI− and by CHON with a smaller CHONS contribution in ESI+. The most strongly correlated formulas contained 6–12 carbon atoms and exhibited intermediate O/C ratios, defining a moderately oxygenated subset of the tunnel organic aerosol. Their positive correlations show that these organic formulas increased during periods with elevated particulate NH_4^+ and NO_3^-. Gasoline vehicle emissions can supply NH_3 and NO_x precursors relevant to NH_4NO_3 formation in traffic influenced air (Sun et al., 2017; Link et al., 2017). The observed covariance identifies a group of organic formulas associated with NH_4^+/NO_3^- rich tunnel aerosol. Together, the recurrent detection of these formulas and the limited variation in CoreFrac define a consistent molecular baseline of $PM_{2.5}$ in the gasoline dominated tunnel environment for subsequent comparison with the controlled gasoline tailpipe profile.

https://doi.org/10.5194/egusphere-2026-4948
Preprint. Discussion started: 21 August 2026

3.3. CD–Tunnel molecular contrast and tailpipe coverage

To identify differences in molecular formula occurrence between the tunnel and the CD tailpipe profile, detected formulas were grouped within each mode into tunnel only (T–O), CD only (CD–O), and Tunnel-CD Common (TCC). TCC was defined as the intersection of formulas detected in at least one tunnel sample and formulas detected in at least one of the three CD conditions. T–O and CD–O represented the corresponding set differences. (Figure 4a, fractions are by formula number unless otherwise noted). T–O contained more formulas than CD–O in both ESI− (1,108 vs 666) and ESI+ (2,189 vs 1,859), indicating greater formula richness in the tunnel aerosol than in the controlled CD tailpipe profile. Elemental class composition differed among the three groups. In ESI−, T–O contained a higher fraction of sulfur-containing classes than CD–O (46% vs 36%). CD–O showed a higher CHON fraction than T–O in ESI− (40% vs 27%), and this enrichment persisted in ESI+ (33% vs 29%). The higher fraction of sulfur-containing formulas in T–O indicates a chemically distinct sulfur-containing molecular group in tunnel aerosol. This composition is consistent with additional traffic-related inputs and chemical processing within the tunnel. In contrast, CD–O was enriched in CHON formulas preferentially detected in the controlled tailpipe exhaust. In addition, TCC (312 formulas in ESI− and 1,089 in ESI+) accounted for one-third to two-thirds of the total peak area and maintained a consistent elemental class profile within each ionization mode. These results distinguish a CHO/CHON dominated molecular baseline shared by the tunnel and controlled tailpipe profiles from a tunnel retained group with a higher fraction of sulfur-containing formulas.

The tailpipe coverage ratio (TCR) was calculated separately within each ionization mode and elemental class as TCC peak area divided by the sum of TCC and T–O peak areas (Figure 4b). For each ionization mode and elemental class, TCR was calculated from pooled blank-corrected peak areas across all 28 tunnel samples, with non-detects treated as zero. TCR therefore quantifies the fraction of the tunnel associated HRMS peak area assigned to formulas also detected in the controlled single vehicle tailpipe profile. CHO and CHON showed high TCR values in both ESI+ (0.77 and 0.84) and ESI− (0.82 and 0.92). In contrast, CHOS and CHONS showed lower TCR values of 0.09 and 0.22 in ESI+ and 0.17 and 0.07 in ESI−. The combined sulfur containing TCR was 0.15 in ESI+ and 0.10 in ESI−. KMD network analysis identified 190 sulfur containing homologous series with at least three members, comprising 81 CH_2 series, 78 C_2H_4 series, and 31 O addition series (Figure S4). Thirty six series contained no TCC or CD–O member and were composed exclusively of T–O formulas or candidate formulas associated with tire wear products. Among the CH_2 series, 18 of 81 met this criterion and formed horizontal alignments in KMD space. Together with the low TCR values of CHOS and CHONS, these results show that part of the tunnel retained sulfur containing composition occurred as organized formula families outside TCC.

https://doi.org/10.5194/egusphere-2026-4948
Preprint. Discussion started: 21 August 2026

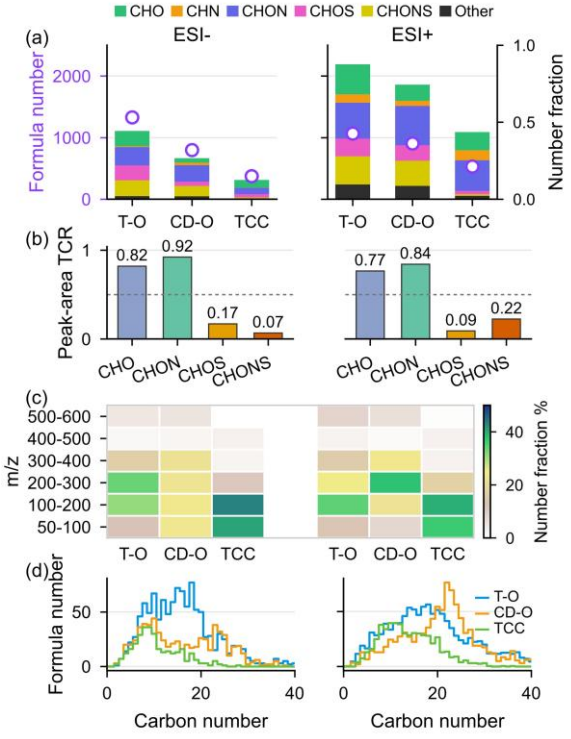

Figure 4. Molecular formula characteristics of tunnel-only (T–O), CD only (CD–O), and Tunnel–CD Common (TCC) formulas in ESI− and ESI+. (a) Formula number and number fraction by elemental class. (b) Tailpipe coverage ratio (TCR), calculated from tunnel peak areas as TCC/(TCC + T–O). (c) Formula number fractions across *m/z* bins. (d) Carbon number distributions by detection category.

The *m/z* and carbon number distributions further resolved this molecular contrast (Figure 4c,d). TCC occurred mainly at *m/z* ≤200 (34%), while T–O was centered at *m/z* 100–300 (65%) across both modes. CD–O exhibited a higher m/z distribution, predominantly at *m/z* 300–500 in ESI+, relative to T–O and TCC. In ESI−, CD–O showed a bimodal carbon number distribution with modes at C_{10} and C_{23} and a pronounced contribution from $C_{18–26}$. T–O was unimodal with a mid-chain maximum near C_{18}, and TCC remained concentrated at low to intermediate carbon numbers. In ESI+, CD–O contained a larger long-chain fraction (nC ≥25), T–O broadened toward C_{15}–C_{30}, and TCC again occupied lower carbon numbers. These distributions indicate that CD–O is enriched in longer-chain species consistent with fresh tailpipe emissions, whereas T–O emphasizes mid-chain constituents consistent with additional tunnel inputs and near-road processing. TCC represents a low-mass, low to mid-chain subset present in both environments.

A reference guided selection was used to examine whether formulas retained in the tunnel were compositionally associated with reported tire rubber additives and their transformation products (Figure 5). The molecular formulas of 6PPD, 2-

https://doi.org/10.5194/egusphere-2026-4948
Preprint. Discussion started: 21 August 2026

aminobenzothiazole (ABT), and 2-phenylbenzothiazole (PhBT) were used as Primary TWP reference compositions, whereas those of 6PPD quinone and 2-hydroxybenzothiazole (2-OH-BTH) were used as Secondary TWP reference compositions (Seiwert et al., 2022; Klöckner et al., 2020). Candidate selection combined tunnel detection frequency, correlation with the reference formulas, elemental constraints, and CH_2 based KMD coherence, as detailed in the Supporting Information. This procedure yielded 62 Primary TWP candidates and 24 Secondary TWP candidates. Primary TWP candidates showed greater unsaturation and were dominated by CHON (41.9%) and CHN (33.9%), whereas Secondary candidates comprised CHON (83.3%) and CHONS (16.7%). Both groups occurred primarily at *m/z* 100–300 and C_8–C_{22}. Approximately 56% of the Primary TWP candidates and 54% of the Secondary TWP candidates occurred in CH_2 spaced homologous series. Representative series associated with the reference compositions included $C_7H_6N_2S$-$(CH_2)_n$ for ABT, $C_{10}H_8N_2$-$(CH_2)_n$ for 6PPD, $C_{12}H_{10}N_2O_2$-$(CH_2)_n$ for 6PPD-quinone, and $C_{13}H_9NS$-$(CH_2)_n$ for PhBT. The regular CH_2 increments indicate that these candidate formulas were organized into homologous molecular families and provide a compositional basis for examining their distribution among the HCA domains.

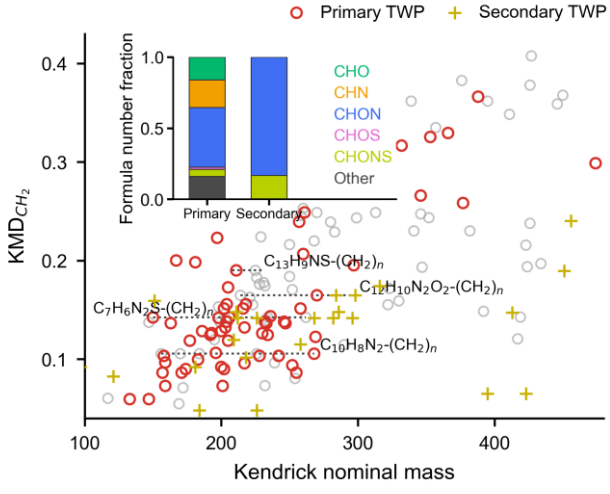

Figure 5. CH_2-based Kendrick mass defect map for candidate formulas associated with tire wear. Gray open symbols denote formulas outside KMD series, and colored symbols denote members of CH_2 spaced formula series. Inset bars show elemental class number fractions for formulas associated with primary tire wear reference compounds and transformation product reference compounds.

https://doi.org/10.5194/egusphere-2026-4948
Preprint. Discussion started: 21 August 2026

3.4. Molecular complexity of traffic aerosol beyond controlled gasoline tailpipe emissions

To resolve molecular domains shared between the controlled chassis dynamometer tailpipe profile and tunnel aerosol, as well as those retained predominantly in the tunnel, HCA was applied to 709 formula assignments selected by volcano screening after all 28 tunnel samples were included. All 709 assignments had Benjamini–Hochberg-adjusted $q < 0.10$ within their respective ionization modes, and 698 met $q < 0.05$. ESI+ contributed 626 assignments (88.3%), including 62 of the 63 candidate TWP assignments, whereas ESI− contributed 83 assignments. In the mutually exclusive post-clustering annotation, T–O accounted for 65.2% of the HCA input, followed by TCC (15.2%), CCO (10.7%), and the combined Primary TWP and Secondary TWP candidate categories (8.9%). The selected $K = 3$ and $\alpha = 0.80$ partition resolved C1, C2, and C3 with 585, 74, and 50 assignments, respectively. The partition had a mean silhouette coefficient of 0.622, a median silhouette coefficient of 0.729, and a negative silhouette fraction of 4.2%. Sensitivity analyses for K and α are provided in the Supporting Information. Among the three HCA domains, C1 was the largest domain, containing 585 assignments and accounting for 82.5% of the HCA input. It contained 162 of the 184 TCC and CCO assignments identified across the complete HCA dataset, showing that most formulas shared with the controlled tailpipe profile occurred within this domain. Within ESI+ and ESI−, TCC and CCO together contributed 62.4% and 84.2% of the C1 peak area, respectively. At the same time, 376 C1 assignments (64.3%) were classified as T–O, demonstrating substantial formula level expansion of this composition in the tunnel samples. CHO and CHON represented 60.9% of the C1 assignments, close to their combined formula number fractions in the controlled tailpipe profile (57.4% in ESI+ and 57.8% in ESI−). The broad m/z and Van Krevelen distributions extended from reduced to moderately oxygenated compositions. A median $\overline{OS}_c$ of −1.07 and median AI_{mod} of 0.29 indicate a predominantly reduced composition with low modified aromaticity. These results identify C1 as the principal CHO/CHON rich molecular baseline connecting the controlled gasoline tailpipe and tunnel profiles, while its large T–O fraction records additional molecular diversity under tunnel conditions.

Compared with C1, C2 and C3 contained larger proportions of formulas detected only in the tunnel and smaller TCC contributions. C2 contained 74 assignments, including 55 T–O assignments (74.3%), 13 TCC assignments (17.6%), and six candidate formulas associated with reported tire wear chemicals (8.1%). CHOS and CHONS comprised 52.7% of C2, including 32 CHONS and seven CHOS assignments. This composition was also evident in the mode specific peak area distributions, in which CHOS and CHONS accounted for 62.4% of C2 peak area in ESI+ and 48.6% in ESI−. The agreement between assignment number and peak area demonstrates that the organosulfur composition extended across C2 and was not produced solely by a few high response assignments. Sulfur atom number was not included in the HCA chemical descriptors; consequently, the separation of these formulas arose from similarities in their day-of-week mean profiles, O/C, H/C, and carbon number. C2 occupied a low to moderate O/C range with a broad H/C distribution and had a median $\overline{OS}_c$ of −1.19 and a median AI_{mod} of 0.22, characterizing it as a reduced organosulfur composition with relatively low modified aromaticity. Together with the low tailpipe coverage ratios of CHOS and CHONS, these results identify C2 as a molecular domain rich in sulfur-containing formulas and characteristic of tunnel aerosol. Its composition is consistent with sulfur-containing traffic materials and chemical

https://doi.org/10.5194/egusphere-2026-4948
Preprint. Discussion started: 21 August 2026

355 processing within the tunnel, with organics associated with lubricants and additives representing plausible contributors (Sonntag et al., 2012; Worton et al., 2014).

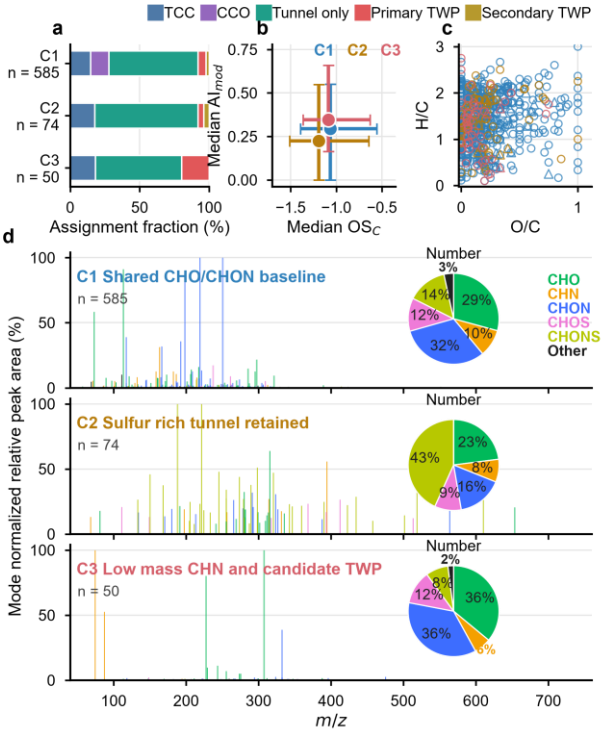

Figure 6. (a) Occurrence category composition of C1–C3 calculated by assignment number. T–O denotes assignments
360 **detected only in tunnel samples, TCC denotes assignments common to the tunnel and controlled tailpipe profiles, and CCO denotes the subset of common assignments whose neutral formulas belonged to the persistent tunnel core. TCC and CCO are displayed as mutually exclusive categories. Primary TWP and Secondary TWP denote candidate formulas associated with reported tire wear compounds and their transformation products, respectively. (b) Structural summary based on peak area weighted carbon oxidation state ($\overline{OS}_c$) and modified aromaticity index (AI_{mod}). Symbols**
365 **show domain medians, and horizontal and vertical bars show interquartile ranges. (c) Van Krevelen distribution colored by HCA domain. Circles and triangles denote ESI+ and ESI− assignments, respectively. (d) Domain resolved mass spectra colored by elemental family. Peak heights represent mean normalized peak areas and were scaled separately to the base peak within each domain and ionization mode before the ESI+ and ESI− spectra were overlaid. Inset pie charts show elemental family composition by assignment number, and *n* indicates the number of assignments**
370 **in each domain.**

https://doi.org/10.5194/egusphere-2026-4948
Preprint. Discussion started: 21 August 2026

C3 contained 50 assignments, including 31 T–O assignments (62.0%), nine TCC assignments (18.0%), and 10 candidate Primary TWP assignments (20.0%). The candidate TWP fraction was more than twice that in C1 (8.0%) and C2 (8.1%), making tire wear associated molecular compositions more prominent in C3 by assignment number. CHO and CHON each accounted for 36.0% of the assignments, sulfur containing formulas accounted for 20.0%, and CHN accounted for 6.0%. C3 comprised 47 ESI+ and only three ESI− assignments; its low molecular mass CHN characteristic was therefore defined primarily by ESI+. Within this mode, $C_4H_{11}N$ accounted for 41.3% of the summed C3 peak area. This formula is consistent with C_4 alkyl amines, including diethylamine reported in air influenced by traffic (Brean et al., 2025). After $C_4H_{11}N$ was excluded and HCA was repeated, all 49 remaining C3 assignments remained together, confirming that the domain membership did not depend on this high response assignment. C3 had a median $\overline{OS}_c$ of −1.09 and the highest median AI_{mod} among the three domains (0.35). Neither nitrogen atom number nor the candidate TWP classification was included in the HCA distance matrix. Their concentration within C3 therefore reflects similarities in temporal behavior and in the O/C, H/C, and carbon number descriptors. C3 therefore represents a distinct molecular domain in tunnel aerosol, characterized by a pronounced low molecular mass CHN response together with an enrichment of candidate formulas associated with reported tire wear compounds. Together with its limited overlap with the controlled tailpipe profile, these characteristics distinguish C3 from the dominant CHO/CHON molecular baseline represented by C1.

Taken together, molecular correspondence between the controlled gasoline tailpipe and tunnel profiles was dominated by the large CHO/CHON-rich C1 baseline, whereas C2 and C3 represented compositionally distinct molecular domains enriched in tunnel aerosol. Because C1 accounted for 82.5% of the selected assignments, comparisons based on overall profile similarity would largely reflect this shared composition and provide limited resolution of the smaller C2 and C3 domains. These results indicate that the controlled gasoline tailpipe profile captured the dominant shared CHO/CHON molecular baseline but incompletely represented the sulfur-rich and other chemically distinct molecular domains present in tunnel aerosol. Comprehensive molecular characterization of traffic $PM_{2.5}$ therefore requires controlled tailpipe measurements together with tunnel or on-road molecular profiles and reference materials representing lubricants, tire wear, road dust, and near-road transformation processes. The organosulfur formulas defining C2 and the candidate TWP-related formulas together with the low molecular mass CHN group characterizing C3 provide specific molecular targets for developing and validating these complementary traffic aerosol reference profiles.

4 Summary and implications

Tunnel $PM_{2.5}$ contained a broader range of assigned molecular formulas than the controlled single vehicle gasoline tailpipe molecular profile. The extent of tailpipe coverage varied markedly among elemental classes. CHO and CHON formulas showed relatively high tailpipe coverage ratios, whereas CHOS and CHONS formulas showed low coverage and were concentrated in tunnel retained domains. HCA further organized the volcano selected assignments into a large C1 domain dominated by the CHO/CHON composition shared between the two profiles, a sulfur rich C2 domain, and a C3 domain

https://doi.org/10.5194/egusphere-2026-4948
Preprint. Discussion started: 21 August 2026

containing candidate TWP formulas and a prominent low molecular mass CHN response in ESI+. Together, the TCR and HCA results show that the controlled gasoline tailpipe profile captured the dominant shared CHO/CHON molecular baseline but incompletely represented a domain rich in sulfur-containing formulas and another domain enriched in candidate formulas associated with reported tire-wear compounds and characterized by a pronounced low-molecular-mass CHN response. These results highlight the importance of complementing controlled tailpipe measurements with molecular profiles representing non-tailpipe vehicle materials and near-road atmospheric processing when constructing traffic $PM_{2.5}$ reference profiles.

For traffic $PM_{2.5}$ source characterization, controlled tailpipe profiles should therefore be regarded as one component of a broader molecular reference framework rather than a complete representation of traffic aerosol. Real tunnel aerosol integrates tailpipe exhaust, lubricant and additive related material, tire and road wear inputs, resuspended road dust, dilution, gas particle partitioning, and near road chemical processing. As exhaust emissions decrease under tighter controls and fleet electrification, these non exhaust and road associated processes will remain linked to vehicle activity, vehicle weight, tire composition, road surface conditions, and tunnel ventilation (Timmers and Achten, 2016; Fussell et al., 2022). The organosulfur formulas concentrated in C2 and the candidate TWP formulas and low molecular mass CHN assignments in C3 provide specific targets for developing and validating complementary traffic aerosol reference profiles, pending compound level validation. Future work should test these candidates using authentic standards, MS/MS spectra, road dust, tire wear, and lubricating oil reference materials, and should integrate LC-HRMS with GC×GC-MS and targeted LC-MS/MS to quantify molecular burdens and evaluate marker stability across vehicle technologies, driving conditions, and road environments.

Data Availability. The datasets used in this study are available upon request to the corresponding author.

Supplement. The supplement related to this article is available online at: https://doi.org.

Author contributions. YH and JC designed and conceptualized the study. LL, with support from HX, QW, and HS, performed aerosol sampling and field measurements. LL, XZ, YC, and FL contributed to the aerosol chemical analysis and data processing. LL, HX and YH wrote the original draft. All authors revised and approved the manuscript before submission.

Competing interests. The authors declare that they have no conflict of interest.

Financial support. This work was funded by the Open Fund of Shanxi Key Laboratory of Complex Air Pollution Control and Carbon Reduction (SXKLA2026K02), the Natural Science Foundation of Shaanxi Province (2022JQ-250), the Natural Science Basic Research Program of Shaanxi Province (2025JC-YBQN-398 and 2025JC-QYCX-030).

https://doi.org/10.5194/egusphere-2026-4948
Preprint. Discussion started: 21 August 2026

References

Alam, M. S., Zeraati-Rezaei, S., Xu, H., and Harrison, R. M.: Characterization of gas and particulate phase organic emissions (C_9–C_{37}) from a diesel engine and the effect of abatement devices, Environmental science & technology, 53, 11345–11352, 10.1021/acs.est.9b03053, 2019.

Banerjee, S. and Mazumdar, S.: Electrospray ionization mass spectrometry: a technique to access the information beyond the molecular weight of the analyte, International journal of analytical chemistry, 2012, 282574, 10.1155/2012/282574, 2012.

Boogaard, H., Patton, A., Atkinson, R., Brook, J., Chang, H., Crouse, D., Fussell, J., Hoek, G., Hoffmann, B., and Kappeler, R.: Long-term exposure to traffic-related air pollution and selected health outcomes: A systematic review and meta-analysis, Environment international, 164, 107262, 10.1016/j.envint.2022.107262, 2022.

Brean, J., Bortolussi, F., Rowell, A., Beddows, D. C., Weinhold, K., Mettke, P., Merkel, M., Kumar, A., Barua, S., and Iyer, S.: Traffic-Emitted Amines Promote New Particle Formation at Roadsides, ACS ES&T Air, 2, 1704–1713, 10.1021/acsestair.5c00119, 2025.

Cai, D., Wang, X., George, C., Cheng, T., Herrmann, H., Li, X., and Chen, J.: Formation of secondary nitroaromatic compounds in polluted urban environments, Journal of Geophysical Research: Atmospheres, 127, e2021JD036167, 10.1029/2021jd036167, 2022.

Cech, N. B. and Enke, C. G.: Practical implications of some recent studies in electrospray ionization fundamentals, Mass spectrometry reviews, 20, 362–387, 10.1002/mas.10008, 2001.

Cui, M., Li, C., Chen, Y., Zhang, F., Li, J., Jiang, B., Mo, Y., Li, J., Yan, C., and Zheng, M.: Molecular characterization of polar organic aerosol constituents in off-road engine emissions using Fourier transform ion cyclotron resonance mass spectrometry (FT-ICR MS): implications for source apportionment, Atmospheric Chemistry and Physics, 19, 13945–13956, 10.5194/acp-19-13945-2019, 2019.

Cunha-Lopes, I., Lehtoranta, K., Almeida, S., Evtyugina, M., Vicente, A., Vicente, E., Kuutti, H., Amato, F., and Alves, C.: Chemical speciation of PM emissions from heavy-duty vehicles, Atmospheric Environment, 306, 119823, 10.1016/j.atmosenv.2023.119823, 2023.

Fang, H., Huang, X., Xiao, S., Lowther, S., Fu, X., Zhang, Y., Wu, T., Hu, W., Zhang, G., and Ding, X.: Intermediate-volatility organic compounds observed in a coastal megacity: Importance of non-road source emissions, Journal of Geophysical Research: Atmospheres, 127, e2022JD037301, 10.1029/2022jd037301, 2022.

Fussell, J. C., Franklin, M., Green, D. C., Gustafsson, M., Harrison, R. M., Hicks, W., Kelly, F. J., Kishta, F., Miller, M. R., and Mudway, I. S.: A review of road traffic-derived non-exhaust particles: emissions, physicochemical characteristics, health risks, and mitigation measures, Environmental science & technology, 56, 6813–6835, 2022.

Hartikainen, A. H., Ihalainen, M., Yli-Pirilä, P., Hao, L., Kortelainen, M., Pieber, S. M., and Sippula, O.: Photochemical transformation and secondary aerosol formation potential of Euro6 gasoline and diesel passenger car exhaust emissions,

https://doi.org/10.5194/egusphere-2026-4948
Preprint. Discussion started: 21 August 2026

Journal of Aerosol Science, 171, 106159, 10.1016/j.jaerosci.2023.106159, 2023.

He, X., Zheng, X., Jiang, B., Cao, X., Chen, T., Guo, S., Li, Z., Ding, Y., Zhang, S., and Cheng, Y.: Significant N-containing brown carbon emission from heavy-duty diesel vehicles revealed by the molecular and chromophore analysis using ultra-high resolution mass spectrometry, npj Climate and Atmospheric Science, 8, 200, 10.1038/s41612-025-01034-8, 2025.

Heydari, S., Tainio, M., Woodcock, J., and de Nazelle, A.: Estimating traffic contribution to particulate matter concentration in urban areas using a multilevel Bayesian meta-regression approach, Environment international, 141, 105800, 10.1016/j.envint.2020.105800, 2020.

Jiang, N., Li, M., Wang, Z., Hao, X., Guo, Z., Guo, J., Zhang, R., Zhang, H., Chen, J., and Geng, N.: P-phenylenediamines (PPDs) and 6PPD-quinone in tunnel $PM_{2.5}$: From the perspective of characterization, emission factors, and health risks, Journal of Hazardous Materials, 480, 136269, 10.1016/j.jhazmat.2024.136269, 2024.

Kendrick, E.: A mass scale based on CH_2=14.0000 for high resolution mass spectrometry of organic compounds, Analytical Chemistry, 35, 2146–2154, 10.1021/ac60206a048, 1963.

Kim, Y., Sartelet, K., Seigneur, C., Charron, A., Besombes, J.-L., Jaffrezo, J.-L., Marchand, N., and Polo, L.: Effect of measurement protocol on organic aerosol measurements of exhaust emissions from gasoline and diesel vehicles, Atmospheric Environment, 140, 176–187, 10.1016/j.atmosenv.2016.05.045, 2016.

Kind, T. and Fiehn, O.: Seven Golden Rules for heuristic filtering of molecular formulas obtained by accurate mass spectrometry, BMC Bioinformatics, 8, 1–20, 10.1186/1471-2105-8-105, 2007.

Klöckner, P., Seiwert, B., Eisentraut, P., Braun, U., Reemtsma, T., and Wagner, S.: Characterization of tire and road wear particles from road runoff indicates highly dynamic particle properties, Water Research, 185, 116262, 10.1016/j.watres.2020.116262, 2020.

Koch, B. P. and Dittmar, T.: From mass to structure: An aromaticity index for high-resolution mass data of natural organic matter, Rapid communications in mass spectrometry, 20, 926–932, 10.1002/rcm.2386, 2006.

Kroll, J. H., Donahue, N. M., Jimenez, J. L., Kessler, S. H., Canagaratna, M. R., Wilson, K. R., Altieri, K. E., Mazzoleni, L. R., Wozniak, A. S., and Bluhm, H.: Carbon oxidation state as a metric for describing the chemistry of atmospheric organic aerosol, Nature chemistry, 3, 133–139, 10.1038/nchem.948, 2011.

Lei, Y., Wang, Z., Xu, H., Feng, R., Zhang, N., Zhang, Y., Du, W., Zhang, Q., Wang, Q., and Li, L.: Characteristics and health risks of parent, alkylated, and oxygenated PAHs and their contributions to reactive oxygen species from $PM_{2.5}$ vehicular emissions in the longest tunnel in downtown Xi'an, China, Environmental Research, 212, 113357, 10.1016/j.envres.2022.113357, 2022.

Li, L., Han, Y., Li, J., Lin, Y., Zhang, X., Wang, Q., and Cao, J.: Effects of photochemical aging on the molecular composition of organic aerosols derived from agricultural biomass burning in whole combustion process, Science of The Total Environment, 946, 174152, 10.1016/j.scitotenv.2024.174152, 2024a.

Li, L., Li, J., Zhang, X., Lin, Y., Wang, R., Cao, J., and Han, Y.: Effects of relative humidity on atmospheric organosulfur

https://doi.org/10.5194/egusphere-2026-4948
Preprint. Discussion started: 21 August 2026

species derived from photooxidation and nocturnal chemistry in a forest environment, Environmental Pollution, 363, 125253, 10.1016/j.envpol.2024.125253, 2024b.

Lin, Y., Han, Y., Li, G., Wang, Q., Zhang, X., Li, Z., Li, L., Prévôt, A. S., and Cao, J.: Molecular Characteristics of Atmospheric Organosulfates during Summer and Winter Seasons in Two Cities of Southern and Northern China, Journal of Geophysical Research: Atmospheres, 127, e2022JD036672, 10.1029/2022JD036672, 2022.

Link, M. F., Kim, J., Park, G., Lee, T., Park, T., Babar, Z. B., Sung, K., Kim, P., Kang, S., and Kim, J. S.: Elevated production of NH4NO3 from the photochemical processing of vehicle exhaust: Implications for air quality in the Seoul Metropolitan Region, Atmospheric Environment, 156, 95–101, 10.1016/j.atmosenv.2017.02.031, 2017.

Ministry of Public Security of the People's Republic of China: National motor vehicle ownership reaches 453 million and the number of drivers reaches 542 million, https://www.gov.cn/lianbo/bumen/202501/content_6999762.htm (last access: 14 July 2026), 2025.

Paul, A., Fang, Z., Martens, P., Mukherjee, A., Jakobi, G., Ihalainen, M., Kortelainen, M., Somero, M., Yli-Pirilä, P., and Hohaus, T.: Formation of secondary aerosol from emissions of a Euro 6d-compliant gasoline vehicle with a particle filter, Environmental Science: Atmospheres, 4, 802–812, 10.1039/D3EA00165B, 2024.

Pieber, S. M., Kumar, N. K., Klein, F., Comte, P., Bhattu, D., Dommen, J., Bruns, E. A., Kılıç, D., El Haddad, I., and Keller, A.: Gas-phase composition and secondary organic aerosol formation from standard and particle filter-retrofitted gasoline direct injection vehicles investigated in a batch and flow reactor, Atmospheric Chemistry and Physics, 18, 9929–9954, 10.5194/acp-18-9929-2018, 2018.

Pirjola, L., Karjalainen, P., Heikkila, J., Saari, S., Tzamkiozis, T., Ntziachristos, L., Kulmala, K., Keskinen, J., and Ronkko, T.: Effects of fresh lubricant oils on particle emissions emitted by a modern gasoline direct injection passenger car, Environmental science & technology, 49, 3644–3652, 10.1021/es505109u, 2015.

Platt, S. M., El Haddad, I., Zardini, A. A., Clairotte, M., Astorga, C., Wolf, R., Slowik, J. G., Temime-Roussel, B., Marchand, N., and Ježek, I.: Secondary organic aerosol formation from gasoline vehicle emissions in a new mobile environmental reaction chamber, Atmospheric Chemistry and Physics, 13, 9141–9158, 10.5194/acp-13-9141-2013, 2013.

Rudnick, L. R., Ed: Lubricant additives: chemistry and applications, 3rd ed.; CRC Press: Boca Raton, FL, 10.1201/9781315120621, 2017.

Schneider, E., Czech, H., Hartikainen, A., Hansen, H. J., Gawlitta, N., Ihalainen, M., Yli-Pirilä, P., Somero, M., Kortelainen, M., and Louhisalmi, J.: Molecular composition of fresh and aged aerosols from residential wood combustion and gasoline car with modern emission mitigation technology, Environmental Science: Processes & Impacts, 26, 1295–1309, 10.1039/d4em00106k, 2024.

Seiwert, B., Nihemaiti, M., Troussier, M., Weyrauch, S., and Reemtsma, T.: Abiotic oxidative transformation of 6-PPD and 6-PPD quinone from tires and occurrence of their products in snow from urban roads and in municipal wastewater, Water Research, 212, 118122, 10.1016/j.watres.2022.118122, 2022.

Shafer, M. M., Overdier, J. T., and Schauer, J. J.: Particle-size resolved aerosol levels of total and extractable platinum in

https://doi.org/10.5194/egusphere-2026-4948
Preprint. Discussion started: 21 August 2026

urban and rural regions of Western Europe, Atmospheric Environment, 318, 120213, 10.1016/j.atmosenv.2023.120213, 2024.

Sonntag, D. B., Bailey, C. R., Fulper, C. R., and Baldauf, R. W.: Contribution of lubricating oil to particulate matter emissions from light-duty gasoline vehicles in Kansas City, Environmental science & technology, 46, 4191–4199, 10.1021/es203747f, 2012.

Sun, K., Tao, L., Miller, D. J., Pan, D., Golston, L. M., Zondlo, M. A., Griffin, R. J., Wallace, H. W., Leong, Y. J., and Yang, M. M.: Vehicle emissions as an important urban ammonia source in the United States and China, Environmental Science & Technology, 51, 2472–2481, 10.1021/acs.est.6b02805, 2017.

Tang, J., Li, J., Su, T., Han, Y., Mo, Y., Jiang, H., Cui, M., Jiang, B., Chen, Y., and Tang, J.: Molecular compositions and optical properties of dissolved brown carbon in biomass burning, coal combustion, and vehicle emission aerosols illuminated by excitation–emission matrix spectroscopy and Fourier transform ion cyclotron resonance mass spectrometry analysis, Atmospheric Chemistry and Physics, 20, 2513–2532, 10.5194/acp-20-2513-2020, 2020.

Tian, L., Zhao, S., Zhang, R., Lv, S., Chen, D., Li, J., Jones, K. C., Sweetman, A. J., Peng, P. a., and Zhang, G.: Tire wear chemicals in the urban atmosphere: significant contributions of tire wear particles to $PM_{2.5}$, Environmental Science & Technology, 58, 16952–16961, 10.1021/acs.est.4c04378, 2024.

Timmers, V. R. and Achten, P. A.: Non-exhaust PM emissions from electric vehicles, Atmospheric environment, 134, 10–17, 10.1016/j.atmosenv.2016.03.017, 2016.

Tong, H., Kourtchev, I., Pant, P., Keyte, I. J., O'Connor, I. P., Wenger, J. C., Pope, F. D., Harrison, R. M., and Kalberer, M.: Molecular composition of organic aerosols at urban background and road tunnel sites using ultra-high resolution mass spectrometry, Faraday Discussions, 189, 51–68, 10.1039/C5FD00206K, 2016.

Wang, K., Huang, R.-J., Brüggemann, M., Zhang, Y., Yang, L., Ni, H., Guo, J., Wang, M., Han, J., Bilde, M., Glasius, M., and Hoffmann, T.: Urban organic aerosol composition in eastern China differs from north to south: molecular insight from a liquid chromatography-Orbitrap mass spectrometry study, Atmospheric Chemistry and Physics, 21, 9089–9104, 10.5194/acp-21-9089-2021, 2021.

Wang, Y., Hu, M., Wang, Y., Zheng, J., Shang, D., Yang, Y., Liu, Y., Li, X., Tang, R., and Zhu, W.: The formation of nitro-aromatic compounds under high NO_x and anthropogenic VOC conditions in urban Beijing, China, Atmospheric Chemistry and Physics, 19, 7649–7665, 10.5194/acp-19-7649-2019, 2019.

Worton, D. R., Isaacman, G., Gentner, D. R., Dallmann, T. R., Chan, A. W., Ruehl, C., Kirchstetter, T. W., Wilson, K. R., Harley, R. A., and Goldstein, A. H.: Lubricating oil dominates primary organic aerosol emissions from motor vehicles, Environmental science & technology, 48, 3698–3706, 10.1021/es405375j, 2014.

Wu, T., Li, Z., Yao, J., Chen, H., Xu, R., Yang, X., Wei, Y., and Ding, Y.: Epigenetic mechanisms linking traffic-related organic pollutants to pulmonary damage: insights from tire and brake wear, npj Clean Air, 2, 45, 10.1038/s44407-026-00088-z, 2026.

Xinhua: Xi'an to impose traffic restriction on vehicle use, https://www.xinhuanet.com/english/2019-03/17/c_137901628.htm

https://doi.org/10.5194/egusphere-2026-4948
Preprint. Discussion started: 21 August 2026

(last access: 10 August 2026), 2019.

Xu, H., Li, Y., Feng, R., He, K., Ho, S. S. H., Wang, Z., Ho, K. F., Sun, J., Chen, J., and Wang, Y.: Comprehensive characterization and health assessment of occupational exposures to volatile organic compounds (VOCs) in Xi'an, a major city of northwestern China, Atmospheric Environment, 246, 118085, 10.1016/j.atmosenv.2020.118085, 2021.

Yao, P., Holzinger, R., Materic, D., Oyama, B. S., de Fátima Andrade, M., Paul, D., Ni, H., Noto, H., Huang, R.-J., and Dusek, U.: Methylsiloxanes from vehicle emissions detected in aerosol particles, Environmental science & technology, 57, 14269–14279, 10.1021/acs.est.3c03797, 2023.

Yassine, M. M., Harir, M., Dabek-Zlotorzynska, E., and Schmitt-Kopplin, P.: Structural characterization of organic aerosol using Fourier transform ion cyclotron resonance mass spectrometry: aromaticity equivalent approach, Rapid Commun. Mass Spectrom., 28, 2445–2454, 10.1002/rcm.7038, 2014.

Zhang, J., Peng, J., Song, A., Du, Z., Guo, J., Liu, Y., Yang, Y., Wu, L., Wang, T., and Song, K.: Secondary organic aerosol formation potential from vehicular non-tailpipe emissions under real-world driving conditions, Environmental Science & Technology, 58, 5419–5429, 10.1021/acs.est.3c06475, 2024.

Zhang, X., Li, L., Lin, Y., Wang, R., Zhu, C., Xiao, S., Cao, J., and Han, Y.: Chemical diversity of organosulfur species in various atmospheric environments over the Guanzhong basin of northwest China, Journal of Geophysical Research: Atmospheres, 130, e2024JD042478, 10.1029/2024JD042478, 2025.

Zhong, N., Cao, J., and Wang, Y.: Traffic congestion, ambient air pollution, and health: Evidence from driving restrictions in Beijing, Journal of the Association of Environmental and Resource Economists, 4, 821–856, 10.1086/692115, 2017.

Zuraski, K., Harkins, C., Peischl, J., Coggon, M. M., Stockwell, C. E., Robinson, M. A., Gilman, J., Warneke, C., McDonald, B. C., and Brown, S. S.: On-Road Measurements of Nitrogen Oxides, CO, CO_2, and VOC Emissions in Two Southwestern US Cities, ACS ES&T Air, 2, 589–598, 10.1021/acsestair.4c00316, 2025.